Ceria Nanoparticles Stabilized by Organic Surface Coatings Activate the Lysosome-Autophagy System and Enhance Autophagic Clearance

Wensi Song,[†] Seung Soo Lee,[‡] Marzia Savini,[†] Lauren Popp,[†] Vicki L. Colvin,[†,‡] and Laura Segatori*[,†,§,⊥]

Departments of [†]Chemical and Biomolecular Engineering, [‡]Chemistry, [§]Biochemistry and Cell Biology, and [⊥]Bioengineering, Rice University, Houston, Texas 77005, United States

ABSTRACT Cerium oxide nanoparticles (nanoceria) are widely used in a variety of industrial applications including UV filters and catalysts. The expanding commercial scale production and use of ceria nanoparticles have inevitably increased the risk of release of nanoceria into the environment as well as the risk of human exposure. The use of nanoceria in biomedical applications is also being currently investigated because of its recently characterized antioxidative properties. In this study, we investigated the impact of ceria nanoparticles on the lysosome-autophagy system, the main catabolic pathway that is activated in mammalian cells upon internalization of exogenous material. We tested a battery of ceria nanoparticles functionalized with different types of biocompatible coatings (*N*-acetylglucosamine, polyethylene glycol and polyvinylpyrrolidone) expected to have minimal effect on lysosomal integrity and function. We found that ceria nanoparticles promote activation of the transcription factor EB, a master regulator of lysosomal function and autophagy, and induce upregulation of genes of the lysosome-autophagy system. We further show that the array of differently functionalized ceria nanoparticles tested in this study enhance autophagic clearance of proteolipid aggregates that accumulate as a result of inefficient function of the lysosome-autophagy system. This study provides a mechanistic understanding of the interaction of ceria nanoparticles with the lysosome-autophagy system and demonstrates that ceria nanoparticles are activators of autophagy and promote clearance of autophagic cargo. These results provide insights for the use of nanoceria in biomedical applications, including drug delivery. These findings will also inform the design of engineered nanoparticles with safe and precisely controlled impact on the environment and the design of nanotherapeutics for the treatment of diseases with defective autophagic function and accumulation of lysosomal storage material.

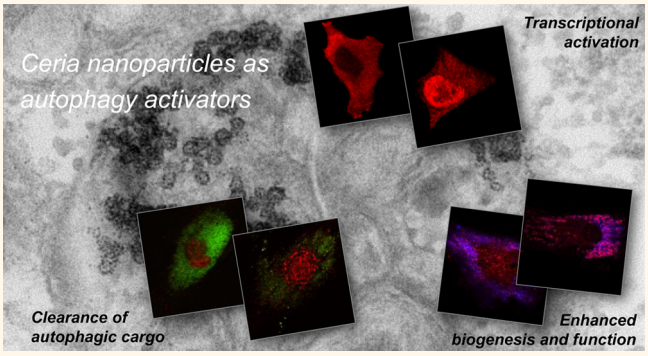

KEYWORDS: cerium oxide nanoparticle · ceria nanoparticle · nanoceria · TFEB · lysosomes · autophagy · lysosomal storage diseases · ceroid lipopigment

Cerium oxide nanoparticles (nanoceria) are used in an increasingly diverse number of applications. The optical properties and ability to filter ultraviolet rays make nanoceria a highly promising material for applications such as UV blockers and filters.[1] Nanosized ceria is also used as catalyst or cocatalyst in a number of reactions, such as water–gas shift, due to its high oxygen storage capacity and high activity in redox reactions.[2,3] Oxygen vacancies are rapidly formed and eliminated by redox cycling between cerium(III) and cerium(IV),[4–6] generating large clusters of Ce^{3+} ion groups exposed to gas reactants that can participate in a range of chemical reactions on the surface of CeO_2.[7–11] It was recently shown that CeO_2 nanoparticles can enhance the combustion of the soot collected on the diesel particulate filters, thus enhancing fuel efficiency and reducing the exhaust emissions when added to diesel fuels.[12–14]

The expanding commercial scale production and use of CeO_2 nanoparticles have inevitably increased the risk of release of nanoceria to the environment as well as the risk of human exposure. Much of the concern associated with the use of nanoceria as

* Address correspondence to segatori@rice.edu.

Received for review July 1, 2014 and accepted October 14, 2014.

Published online October 14, 2014
10.1021/nn505073u

industrial catalyst in fact is related to the potential effects not only on the environment[15] but also on human health.[16−18] On the other hand, recent studies elucidated the antioxidant properties of CeO_2 nanocystals, which were reported to scavenge free radicals or reactive oxygen species (ROS) and protect cells from oxidative stress.[19−22] The antioxidant properties of nanoceria were specifically investigated in light of potential therapeutic implications[23] and, particularly, neuroprotective function.[24] Ceria nanoparticles were shown to function as radical scavengers and protect from radiation-induced cellular damage.[25,26] Furthermore, nanoceria can prevent radical oxygen-induced retinal degeneration.[27,28] Collectively, these findings indicate that nanoceria may provide a promising material for biomedical applications. Evidence of the potential cytotoxic impact of ceria nanoparticles, however, was also reported as CeO_2 nanoparticles were found to lower viability and reduce membrane integrity in human lung cancer cells.[29] CeO_2 nanoparticles were also observed to affect cell viability by inducing activation of apoptosis and autophagic cell death.[18,30−32] However, the molecular mechanism involved in CeO_2-induced activation of these cellular pathways remains unclear.

A variety of engineered nanoparticles,[33−38] including rare earth oxide nanocrystals,[39] once they are internalized into cells, induce activation of autophagy, which is the main catabolic pathway that regulates degradation of aggregated proteins, damaged organelles, and pathogens.[40] Not surprisingly, attempts have been made to identify surface coating peptides that reduce the autophagy inducing properties of engineered nanoparticles.[41] Clearance is mediated by sequestration of intracellular cargo into double-membrane vesicles called autophagosomes.[40] Fusion of autophagosomes with lysosomes, cytoplasmic organelles containing a battery of hydrolytic enzymes, results in the formation of autophagolysosomes where degradation takes place. Increasing evidence suggests that nanoparticles are sequestered into autophagosomes when internalized into cells.[34−36,38,39] However, compartmentalization of nanoparticles into autophagosomes is not necessarily always followed by clearance of autophagosomes by the lysosomes and may result instead in autophagy dysfunction and accumulation of autophagosomes. Gold nanoparticles, for instance, may impair lysosomal function, leading to blockage of the autophagic flux.[42] Moreover, while autophagy is generally considered a prosurvival pathway activated under conditions of stress or starvation, proapoptotic mechanisms can be also induced in association with autophagy activation[43−45] and may be specifically induced upon nanoparticle mediated induction of autophagy.[31,46,47]

Previous evidence suggests that ceria nanoparticles, similar to a number of metal oxide nanomaterials, may impact cellular pathways[29−31,48,49] and, particularly, the autophagy system.[30,31] However, the molecular mechanisms underlying upregulation of the autophagic response upon exposure to ceria nanoparticles are still unclear. In this study, we investigated the impact of ceria nanoparticles on the lysosome-autophagy system with the ultimate goal to understand whether ceria-induced upregulation of autophagy results in coordinated activation of lysosome and autophagosome formation and fusion and consequent increase in autophagic clearance or in blockage of autophagic flux.

Evidence of the integrated and coregulated roles of lysosomes and autophagosomes emerged from the recent discovery of an overarching regulatory gene network (CLEAR, coordinated lysosomal expression and regulation)[50] and its master regulator, the transcription factor EB (TFEB). TFEB regulates the expression of genes encoding lysosomal proteins,[50,51] the processing of lysosomal proteins,[52] and the expression of autophagy genes.[53] This evidence points to the role of TFEB at the crossroad of the regulatory mechanisms that coordinate the autophagy and lysosomal pathways and, importantly, to the function of TFEB as a regulator of autophagic clearance.[54,55]

To test the impact of ceria nanoparticles on the autophagy system we tested a library of ceria nanoparticles of 4.3 $\pm$ 0.5 nm inner core coated with different types of biocompatible coatings: *N*-acetylglucosamine (GlcNAc), polyethylene glycol (PEG) and polyvinylpyrrolidone (PVP). These surface coatings are commonly used in biological and pharmaceutical applications of nanomaterials. For instance, GlcNAc-decorated nanoparticles enhance uptake and delivery of therapeutic molecules both *in vitro* and *in vivo*.[56,57] PEG is widely used to enhance biocompatibility of nanoparticles in biomedical applications[58] and improves brain tissue penetration of large nanoparticles through the brain blood barrier.[59] PVP is a nontoxic, biocompatible material that prevents agglomeration and enhances the blood circulation time of nanoparticles[60] commonly used in MRI contrast agents and drug delivery systems.[61,62] Importantly, the three surface coatings selected in this study represent both negative and neutral interfaces, which do not change acidification of lysosomes or lysosomal integrity.[63] Lysosomal membrane permeabilization is in fact proposed as a potential mechanism of nanoparticle-induced cytotoxicity[64] and was observed in cells exposed to nanoparticles presenting cationic surface modifications that may cause lysosomal rupture through a "proton sponge" effect.[65] Negative and neutral interfaces were thus selected to avoid potential confounding factors and investigate the impact of nanoceria on the autophagy-lysosome system.

To investigate the molecular mechanism of autophagy induction by ceria nanoparticles we used an

in vitro model system of TFEB activation, namely HeLa cells that overexpress TFEB. Inefficient autophagic activity results in aberrant accumulation of intracellular substrates, which may lead to the development of pathologic conditions, such as lysosomal storage disorders.[66,67] Particularly, neuronal ceroid lipofuscinoses (NCL) are a group of more than 12 genetically distinct neurodegenerative lysosomal storage disorders affecting children and young adults.[68,69] The hallmark of this family of diseases is the aberrant intracellular accumulation of autofluorescent ceroid lipopigment.[70] Interestingly, TFEB activation was shown to lower the accumulation of ceroid lipopigment in fibroblasts derived from NCL patients.[71] To investigate the outcome of ceria-mediated induction of autophagy and determine whether it results in enhancement of autophagic clearance, we used fibroblasts derived from a patient with late infantile neuronal ceroid lipofuscinosis (LINCL) that accumulates the autophagic substrate ceroid lipopigment.

We found that all differently functionalized ceria nanoparticles used in this study activate TFEB and enhance autophagic clearance of ceroid lipopigment in LINCL fibroblasts. In summary, this study provides a detailed mechanistic understanding of the impact of ceria nanoparticles on the autophagy system, providing evidence for the first time that cell exposure to nanoceria results in autophagy induction and enhanced clearance of toxic cellular waste.

RESULTS AND DISCUSSION

Synthesis and Characterization of Ceria Nanoparticles. Nanocrystalline CeO_2 were synthesized using the high temperature cerium precursor decomposition method, resulting in nanocrystals with near spherical shape and narrow diameter distribution (D = 4.3 ± 0.5 nm in organic solvents; Figure 1A).[72] CeO_2 nanocrystals capped with oleylamine were first dispersed in hexane due to their hydrophobicity, and subsequently phase transferred into water by the ligand exchange method, using different phase transfer agents (GlcNAc, PEG and PVP). Phase transferred water-soluble CeO_2 nanocrystals presented unaltered morphologies and were colloidally stable as shape and hydrodynamic diameters remained constant for more than six months (data not shown). Representative results obtained using GlcNAc coated CeO_2 (CeO_2−GlcNAc) are reported in Figure 1B,C: phase transferred CeO_2−GlcNAc displayed a 4.3 ± 0.5 nm diameter, as determined using transmission electron microscopy (TEM), and X-ray diffraction (XRD) analyses revealed a cubic fluorite nanocrystal structure. Functionalization with GlcNAc, PEG, and PVP resulted in compact surface coating as shown in Figure 1D. The hydrodynamic diameters of aqueous dispersion of CeO_2 nanocrystals were measured by dynamic light scattering (DLS) (Figure 1D). CeO_2−GlcNAc and CeO_2−PEG200 were found to have small hydrodynamic diameters

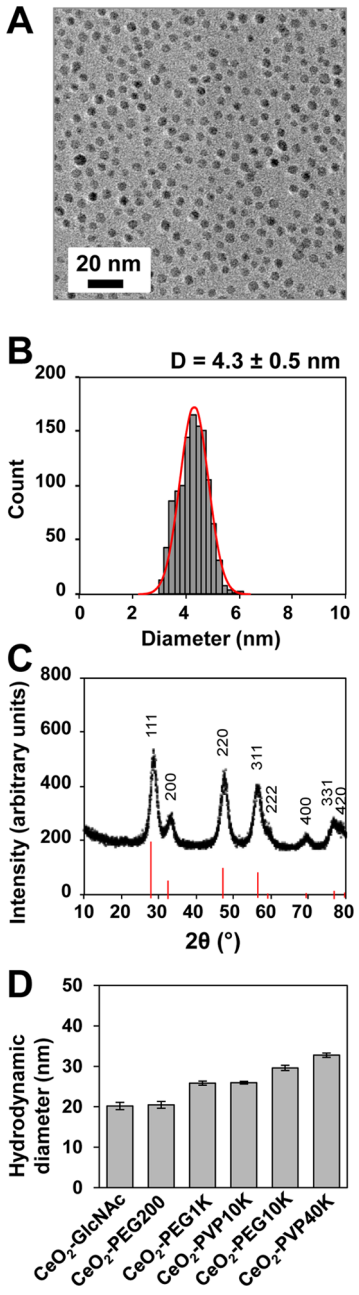

Figure 1. Characterization of ceria nanoparticles. (A) TEM analyses of monodisperse nanocrystals phase transferred to ultrapure water using GlcNAc (scale bar, 20 nm). (B) Size distribution of ceria nanoparticles (CeO_2−GlcNAc) determined by TEM (4.3 ± 0.5 nm). (C) Structure (cubic fluorite) of nanocrystalline cerium oxide verified by XRD; the diffraction patterns (black) match to the reference (JCPDS Card #34−0394 (vertical red lines)). (D) Hydrodynamic diameter of CeO_2 nanoparticles coated with GlcNac, PEG200, PEG1K, PVP10K, PEG10K, PVP40K determined by DLS analyses. Data are reported as mean ± SD (n = 3).

(20.2 ± 0.9 and 20.5 ± 0.8 nm, respectively) due to the low molecular weight of the surface coatings. High molecular weight PEG (PEG1K and 10K) and PVP (PVP10K and 40K) coatings resulted in a larger hydrodynamic diameter (CeO_2−PEG1K: 25.9 ± 0.5 nm; CeO_2−PEG10K: 29.6 ± 0.7 nm; CeO_2−PVP10K: 25.9 ± 0.4 nm; and CeO_2−PVP40K: 32.8 ± 0.5 nm), with the PVP

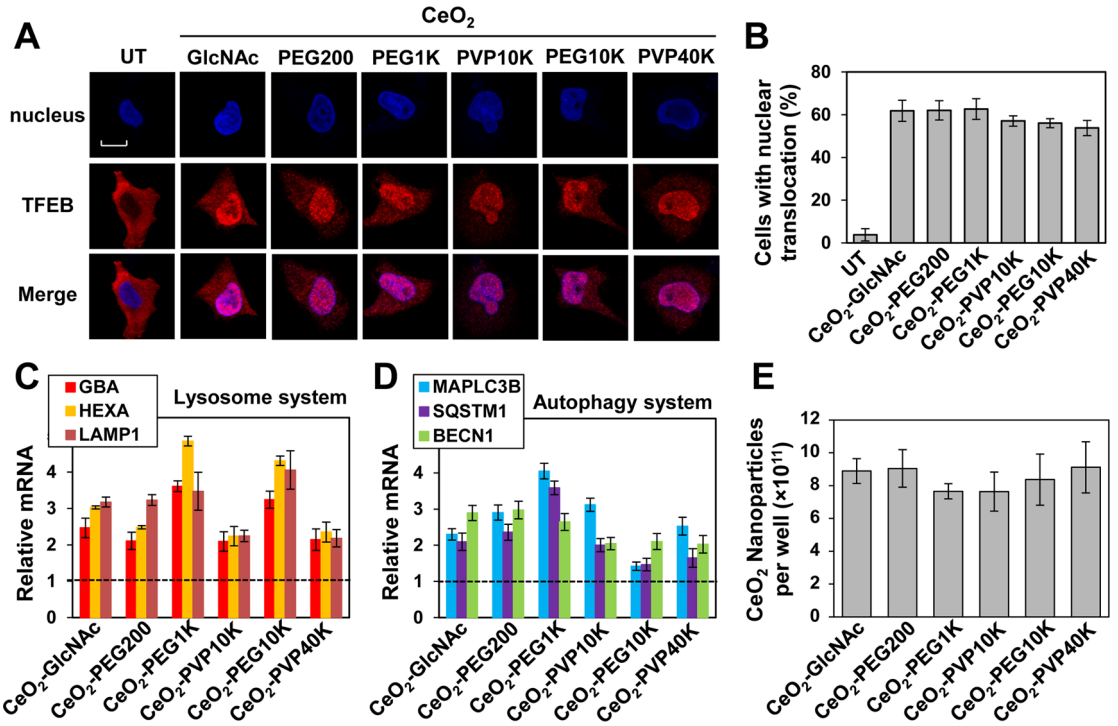

Figure 2. Ceria nanoparticles promote TFEB activation and upregulate the CLEAR network in HeLa/TFEB cells. (A) Confocal microscopy analyses of TFEB subcellular localization in HeLa cells stably transfected with TFEB-3xFLAG treated with 100 ppm of CeO_2 nanoparticles for 24 h. Colocalization of DAPI (blue) and TFEB-3xFLAG (red) is shown in merged images (purple). Representative images are reported. The scale bar is 10 μm. UT, untreated. (B) Percentage of cells with nuclear localization of TFEB-3xFLAG upon nanoceria treatment. Representative fields containing 50−100 cells were analyzed to calculate the percentage of cells with TFEB-3xFLAG nuclear localization in HeLa/TFEB cells ($p < 0.01$). Data are reported as mean ± SD ($n = 3$). UT, untreated. (C) Relative mRNA expression levels of representative genes of the lysosome system in HeLa cells stably transfected with TFEB-3xFLAG treated with 100 ppm of CeO_2 nanoparticles for 24 h. mRNA expression levels of *GBA*, *HEXA*, *LAMP1* were obtained by qRT-PCR, corrected by the expression of the house-keeping gene *GAPDH* and *ACTB*, and normalized to those of untreated cells (dashed line). Data are reported as mean ± SD ($n = 3$; $p < 0.05$). (D) Relative mRNA expression levels of representative genes of the autophagy system in HeLa/TFEB cells treated with 100 ppm of CeO_2 nanoparticles for 24 h. mRNA expression levels of *MAPLC3B*, *SQSTM1*, and *BECN1* were obtained as described in (C). Data are reported as mean ± SD ($n = 3$; $p < 0.05$). (E) Cellular uptake of CeO_2 nanoparticles (100 ppm; 24 h) in HeLa/TFEB cells quantified by ICP-MS.

surface coatings leading to a slightly smaller hydrodynamic diameter compared to the same molecular weight PEG surface coatings because of the wrapping surface structure formed by the PVP coating (compare 25.9 ± 0.4 nm CeO_2−PVP10K to 29.6 ± 0.7 nm CeO_2−PEG10K).[73]

Measurements of the nanoparticles' zeta potentials were conducted to characterize the surface charge of water-soluble ceria nanoparticles. All the surface coatings used resulted in negative to neutral charges (CeO_2−GlcNAc: −13.6 ± 1.5 mV; CeO_2−PEG200: −2.6 ± 1.8 mV; CeO_2−PEG1K: −2.0 ± 1.5 mV; CeO_2−PEG10K: −4.4 ± 2.4 mV; CeO_2−PVP10K: −5.3 ± 1.1 mV; CeO_2−PVP40K: −6.8 ± 3.0 mV), as expected,[74,75] which we hypothesized induce minimal changes on lysosome integrity and function.[63] GlcNAc-coated nanoparticles were found to present the most negatively charged surface due to the presence of acetyl groups and hydroxyl groups on the nanoparticle surface. PEG- and PVP-coated nanoparticles were found to present more neutral surface charges most likely because neither the ether groups of the PEG coating nor the pyrrolidone groups of the PVP coating present a local negative charge.

Ceria Nanoparticles Activate TFEB and Upregulate Cellular Clearance Networks. To investigate whether CeO_2 nanoparticles activate autophagy, we first analyzed the transcriptional regulatory network that controls autophagy activation upon cell treatment with CeO_2 nanocrystals. Specifically, we monitored the transcription factor EB (TFEB), a key hub in the regulation of cellular clearance networks[53] that controls the expression of genes involved in lysosomal biogenesis (the CLEAR network)[51] and autophagy.[55] TFEB localizes predominantly in the cytoplasm in resting cells and translocates into the nucleus upon activation, under conditions that result in enhancement of autophagic activity.[50] To investigate the impact of CeO_2 nanoparticles on TFEB, we first monitored TFEB subcellular localization in a model system of TFEB activation consisting of HeLa cells stably transfected for the expression of TFEB-3xFLAG (HeLa/TFEB cells).[50] Cells were treated with CeO_2 nanocrystals (100 ppm; 24 h) and TFEB intracellular localization was evaluated by confocal microscopy using DAPI nuclear stain and an anti-FLAG antibody (Figure 2A). As expected, TFEB was barely detectable in the nucleus of untreated HeLa/TFEB cells.

Administration of CeO_2 nanoparticles, however, promoted TFEB nuclear localization in cells exposed to CeO_2 nanoparticles coated with GlcNAc, PEG and PVP (Figure 2A). TFEB nuclear localization was quantified by calculating the fraction of HeLa/TFEB cells exposed to CeO_2 nanoparticles that presented nuclear localization of TFEB (Figure 2B). TFEB nuclear localization was observed in 3.8 ± 2.8% of untreated HeLa/TFEB cells. The fraction of cells presenting TFEB nuclear localization was found to increase to over 50% of the total population after 24 h of treatment with the library of CeO_2 nanoparticles (CeO_2−GlcNAc: 61.8 ± 5.0%; CeO_2−PEG200:62.1 ± 4.5%; CeO_2−PEG1K: 62.7 ± 4.8%; CeO_2−PVP10K: 57.1 ± 2.4%; CeO_2−PEG10K: 56.1 ± 2.1%; CeO_2−PVP40K: 53.8 ± 3.5%) (Figure 2B; $p < 0.01$), demonstrating that CeO_2 nanoparticles activate TFEB in HeLa/TFEB cells. Cell treatment with 2-hydroxypropyl-β-cyclodextrin (100 mM; 24 h), a known TFEB activator[76] included here for comparison, resulted in 88.2 ± 1.0% of TFEB nuclear localization (Figure S1, Supporting Information).

To test whether nanoceria-induced nuclear translocation of TFEB results in upregulation of the lysosome system, which is observed upon TFEB activation,[50] we monitored the expression of representative genes of the CLEAR network upon exposure to CeO_2 nanoparticles. HeLa/TFEB cells were treated with CeO_2 nanoparticles (100 ppm; 72 h) and the mRNA expression levels of TFEB targets were monitored by quantitative RT-PCR (qRT-PCR) (Figure 2C). We found that CeO_2 nanoparticles coated with GlcNAc, PEG, and PVP caused significant upregulation of TFEB targets, namely, *GBA* (Glucocerebrosidase; between 2.1- and 3.6-fold), *HEXA* (Hexosaminidase A; between 2.3- and 4.6-fold), and *LAMP1* (Lysosome-associated membrane glycoprotein 1; between 2.2- and 4.1-fold) (Figure 2C; $p < 0.05$).

To test whether CeO_2 nanoparticle-induced activation of TFEB also results in upregulation of the autophagy system, we tested the expression of representative genes involved in different steps of the autophagic pathway. Cells were treated with CeO_2 nanoparticles (100 ppm; 72 h) and mRNA levels were tested by quantitative RT-PCR. We detected upregulation of *MAPLC3*, (microtubule-associated light chain protein 3; between 1.4- and 4.0-fold), which is essential for the formation of autophagic vesicles; *SQSTM1* (p62; between 2.1- and 3.6-fold), which is essential for cargo recognition; and *BECN1* (Beclin-1; between 2.0- and 3.0-fold), which is required for the formation of autophagosomes (Figure 2D; $p < 0.05$). Interestingly, *MAPLC3B* and *SQSTM1* are known to be direct targets of TFEB.[51,53]

Collectively, these results indicate that cell exposure to CeO_2 nanoparticles results in activation of TFEB and transcriptional upregulation of genes involved in autophagy-mediated cellular clearance.

To quantify cellular uptake of CeO_2 nanoparticles used in this study and, particularly, to determine whether the efficiency of cellular uptake affects activation of TFEB and autophagy, we measured the extent of CeO_2 nanoparticle internalization in HeLa/TFEB cells using quantitative inductively coupled plasma mass spectrometry (ICP-MS). Cell growth was not affected by treatment with CeO_2 nanoparticles (100 ppm; 24 h), as determined by cell count (data not shown). Cells were washed with PBS and incubated with acidic solution to remove membrane-binding nanocrystals and allow accurate measurement of intracellular nanocrystal concentration. The concentration of cerium atoms was measured by ICP-MS and the number of CeO_2 nanoparticles internalized by the cells was calculated as described in the Methods. The six differently functionalized CeO_2 nanocrystals were observed to have comparable internalization efficiency, suggesting that the different surface coatings used in this study (GlcNAc, PEG1K and 10K, and PVP10K and 40K) have similar effect on the cellular uptake of CeO_2 nanocrystals (Figure 2E).

Ceria Nanoparticles Activate the Lysosome-Autophagy System. Activation of autophagic clearance may lead to induction of apoptosis,[43−45] suggesting that in addition to a prosurvival function, autophagy may also function as a prodeath pathway. The functional interaction between autophagy and apoptosis is still subject of intense debate.[43−45,77−79] However, evidence suggests that autophagy-associated cell death may result from either excessive induction of apoptosis or blockage of downstream steps of the autophagy pathway.[43−45,80] To investigate whether cell treatment with CeO_2 nanoparticles, under conditions that result in activation of TFEB and transcriptional upregulation of the lysosome-autophagy system, affects the apoptotic pathway, we tested induction of early and late apoptosis in HeLa cells exposed to CeO_2 nanoparticles (100 ppm; 24 h). Particularly, we measured membrane rearrangement, characteristic of early apoptosis (annexin V binding), and membrane fragmentation, characteristic of late apoptosis (propidium iodide (PI) binding), using the Cyto-GLO annexin V-FITC apoptosis detection kit as previously described.[81] None of the CeO_2 nanoparticles tested caused a considerable apoptotic response compared to untreated cells (FITC binding affinity, $p < 0.01$; PI binding population, $p < 0.01$; Figure 3A,B). Taxol (50 nM) was used here as positive control because it is known to stabilize microtubules leading to cell cycle arrest and apoptosis induction.[82] Minimal changes in induction of early apoptosis and no significant changes in induction of late apoptosis were observed after prolonged exposure to the differently functionalized ceria nanoparticles under the same conditions (Figure S2). To confirm that CeO_2 nanoparticles used in this study do not induce cytotoxicity under the conditions resulting in autophagy activation, we measured cell viability and cytotoxicity using LIVE/DEAD Viability/Cytotoxicity Kit. Cells were treated with CeO_2 nanocrystals (100 ppm; 24 h)

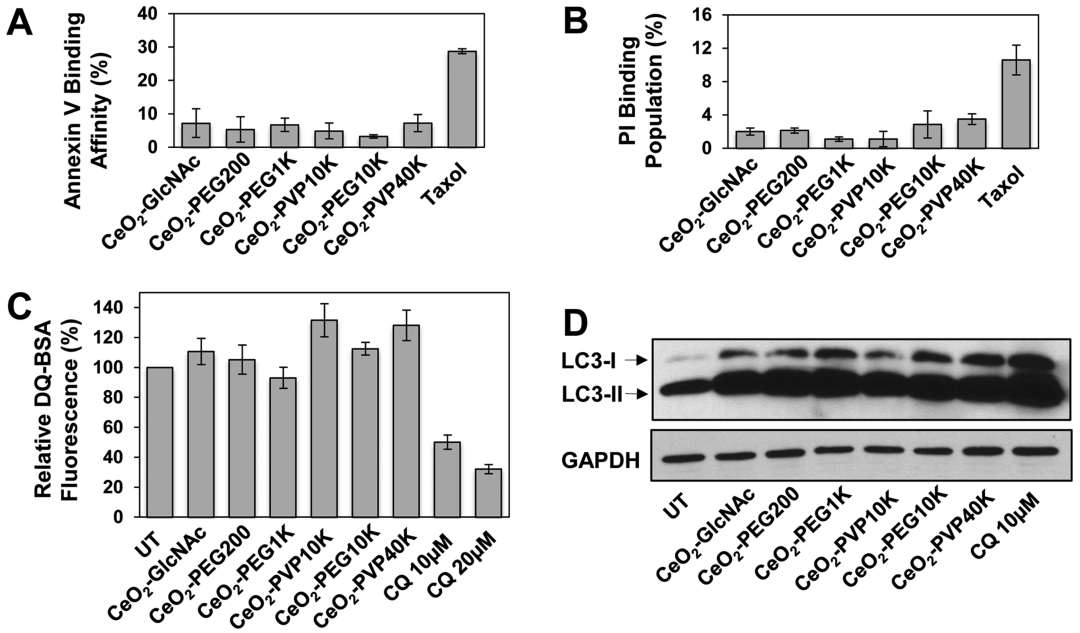

Figure 3. Ceria nanoparticles activate the lysosome-autophagy system. (A) Annexin V binding affinity change (%) in HeLa/TFEB cells treated with CeO_2 nanoparticles (100 ppm) or taxol (50 nM) for 24 h normalized to untreated cells ($p < 0.01$). The results obtained from each replicate were obtained from the analysis of 10 000 cells. Data are reported as the mean ± SD ($n = 3$). (B) Propidium iodide (PI) binding population change (%) of cells treated with CeO_2 nanoparticles (100 ppm) or taxol (50 nM) for 24 h normalized to untreated cells ($p < 0.01$). The results obtained from each replicate were obtained from the analysis of 10 000 cells. Data are reported as the mean ± SD ($n = 3$). (C) Lysosomal activity of HeLa/TFEB cells treated with CeO_2 nanoparticles (100 ppm) or chloroquine (10 μM and 20 μM) for 24 h evaluated using the fluorogenic substrate DQ Green BSA. The results obtained from each replicate were obtained from the analysis of 10 000 cells. Data are reported as mean ± SD ($n = 3$). UT, untreated; CQ, chloroquine. (D) Western blot analyses of LC3 isoforms (cytoplasmic LC3-I and autophagosome-associated LC3-II) in HeLa/TFEB cells treated with CeO_2 nanoparticles (100 ppm) or chloroquine (10 μM) for 24 h, and detected using an LC3 antibody. GAPDH served as loading control. UT, untreated; CQ, chloroquine.

and cell viability was evaluated by confocal microscopy. None of the six differently surface functionalized CeO_2 nanoparticles caused cell death under the conditions used in this study (Figure S3).

These results suggest that the CeO_2 nanoparticles used herein presenting various surface coatings and hydrodynamic diameters (Figure 1D) do not induce activation of apoptosis and cytotoxicity in HeLa/TFEB cells under conditions that result in transcriptional upregulation of autophagy, in agreement with previously reported evidence of low acute cytotoxicity observed under similar conditions.[22,83]

As described above, autophagy-mediated cellular clearance relies on the coordinated activation of lysosome and autophagosome biogenesis and function, which are essential for degradation of autophagic substrates.[84] Hence, not only both branches of the lysosome-autophagy system need to be transcriptionally upregulated, but also need to be functionally active to avoid blockage of the autophagic flux.

Previous studies suggest that depending on the material's charge and composition, nanoparticles may cause impairment of lysosomal function. Under these conditions, transcriptional upregulation of autophagy genes and increased formation of autophagosomes is ultimately associated with decreased autophagic clearance.[42] To investigate the impact of CeO_2 nanoparticles on lysosomal function, we quantified the lysosomal degradation capacity of HeLa/TFEB treated with CeO_2 nanoparticles. Specifically, HeLa/TFEB cells treated with CeO_2 nanoparticles (100 ppm; 24 h) were labeled with the fluorogenic substrate DQ Green BSA, a bovine serum albumin derivative conjugated to the self-quenched dye BODIPY.[85] Proteolysis of DQ-BSA by lysosomal hydrolases results in release of the fluorescent product BODIPY. Therefore, cell fluorescence intensity in this assay is an indication of lysosomal activity. Cells treated with CeO_2 nanocrystals displayed fluorescence intensity comparable to or higher than untreated cell, indicating that none of CeO_2 nanoparticles impairs lysosomal function (Figure 3C). The lysosomal inhibitor chloroquine (CQ; 10 and 20 μM)[86] was used as a control in this study and resulted in decrease in cell fluorescence in a concentration dependent fashion. These results confirm that cell treatment with CeO_2 nanocrystals, under conditions that result in upregulation of the gene network underlying the lysosome-autophagy system, do not impair lysosomal function, which is necessary for productive clearance of autophagic material.

To investigate whether TFEB activation and upregulation of autophagy genes upon exposure to CeO_2 nanoparticles results in altered formation of autophagosomes, we monitored the processing of LC3,

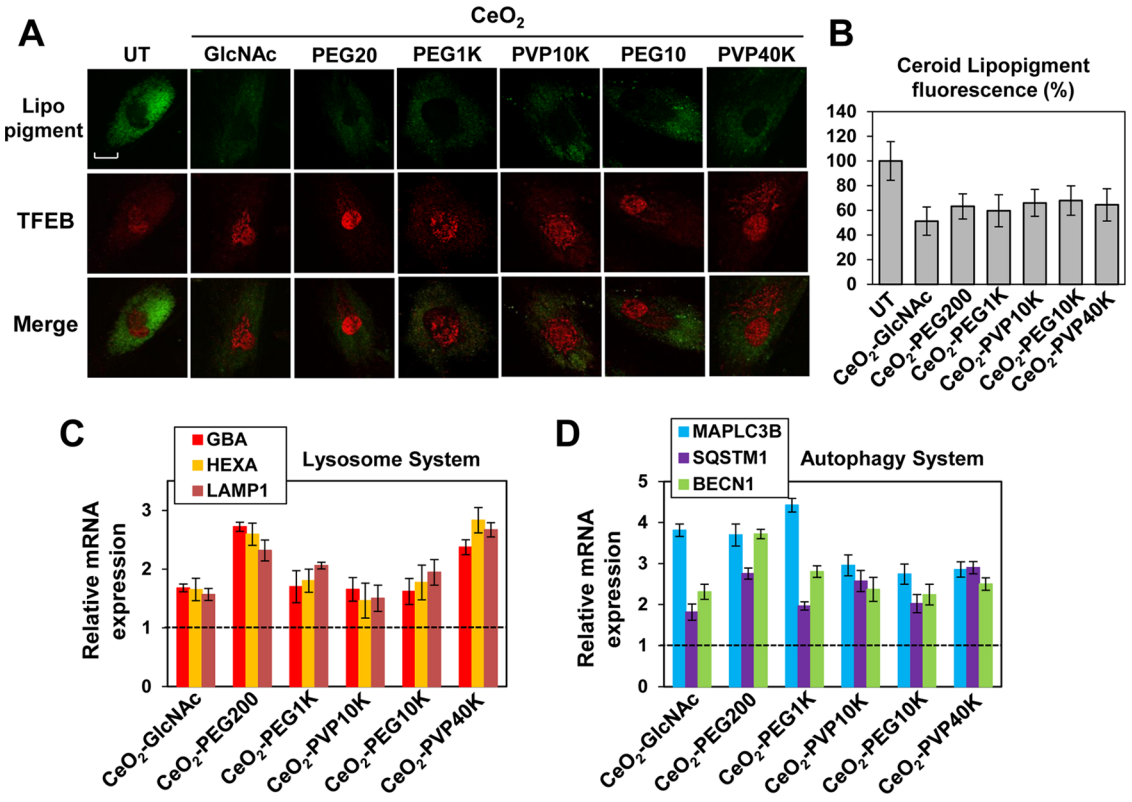

Figure 4. Ceria nanoparticles promote TFEB activation and clearance of ceroid lipopigment in LINCL fibroblasts. (A) Confocal microscopy analyses of ceroid lipopigment (green) and TFEB (red) in LINCL fibroblasts treated with CeO_2 nanoparticles (100 ppm for 3 days) and evaluated by detecting green autofluorescence and binding of anti-TFEB antibody, respectively. The scale bar is 10 μm. UT, untreated. (B) Quantification of ceroid lipopigment fluorescence intensity. Data are reported as mean $\pm$ SD ($n = 15$; $p < 0.01$). UT, untreated. (C) Relative mRNA expression levels of representative genes of the lysosome system in LINCL fibroblasts treated with 100 ppm of CeO_2 nanoparticles for 3 days. mRNA expression levels of *GBA*, *HEXA*, *LAMP1* were obtained as described in Figure 2C. Data are reported as mean $\pm$ SD ($n = 3$; $p < 0.05$). (D) Relative mRNA expression levels of representative genes of the autophagy system in LINCL fibroblasts treated with 100 ppm of CeO_2 nanoparticles for 3 days. mRNA expression levels of *MAPLC3B*, *SQSTM1*, and *BECN1* were obtained as described in Figure 2C. Data are reported as mean $\pm$ SD ($n = 3$; $p < 0.05$).

a protein found on the membrane of autophagosomes[87] and widely used as marker of autophagy activation.[88] Upon activation of autophagy, the cytosolic form of LC3 (LC3-I) is conjugated to phosphatidylethanolamine (LC3-II), which is recruited to autophagosomal membranes.[89] Although the actual molecular weight of LC3-II is larger than that of LC3-I, LC3-II migrates faster than LC3-I on SDS-PAGE due to its hydrophobicity and thus displays a lower apparent molecular weight (14 kDa).[89] LC3-II can be therefore detected and distinguished from LC3-I by Western blot analyses using an LC3-specific antibody.[52] The amount of LC3-II in HeLa/TFEB cells was found to increase upon exposure to CeO_2 nanoparticles (100 ppm; 24 h), indicating that treatment with CeO_2 nanocrystals enhances the formation of autophagic vesicles (Figure 3D).

Taken together, these results confirm that cellular uptake of CeO_2 nanoparticles results in upregulation of the lysosome-autophagy system and does not cause impairment of lysosomal function and consequent activation of autophagy-associated cell death.

Ceria Nanoparticles Promote Autophagic Clearance of Ceroid Lipopigment in LINCL Fibroblasts. A variety of cellular substrates are normally degraded by autophagy and are found to accumulate under pathologic conditions characterized by insufficient autophagic activity.[64] To verify that cell exposure to CeO_2 nanoparticles under conditions that result in activation of TFEB and upregulation of autophagy leads to enhanced cellular clearance, we used an *in vitro* model of accumulation of autophagic cargo. Specifically, we used fibroblasts derived from a patient with late infantile neuronal ceroid lipofuscinosis (LINCL), which are characterized by accumulation of ceroid lipopigment, a lipofuscin-like autofluorescent material.[70] Accumulation of ceroid lipopigment in these cells is caused by mutations in the gene encoding Tripeptidyl peptidase (TPP1), which results in deficiency in TPP1 activity.[76]

To test the effect of CeO_2 nanoparticles on the accumulation of ceroid lipopigment, LINCL fibroblasts were incubated with the different types of CeO_2 nanoparticles (100 ppm for 3 days). Confocal microscopy analyses showed that CeO_2 nanoparticle treatment promotes clearance of ceroid lipopigment as shown by the loss of autofluorescence (Figure 4A, green). The accumulation of autofluorescent material in cells

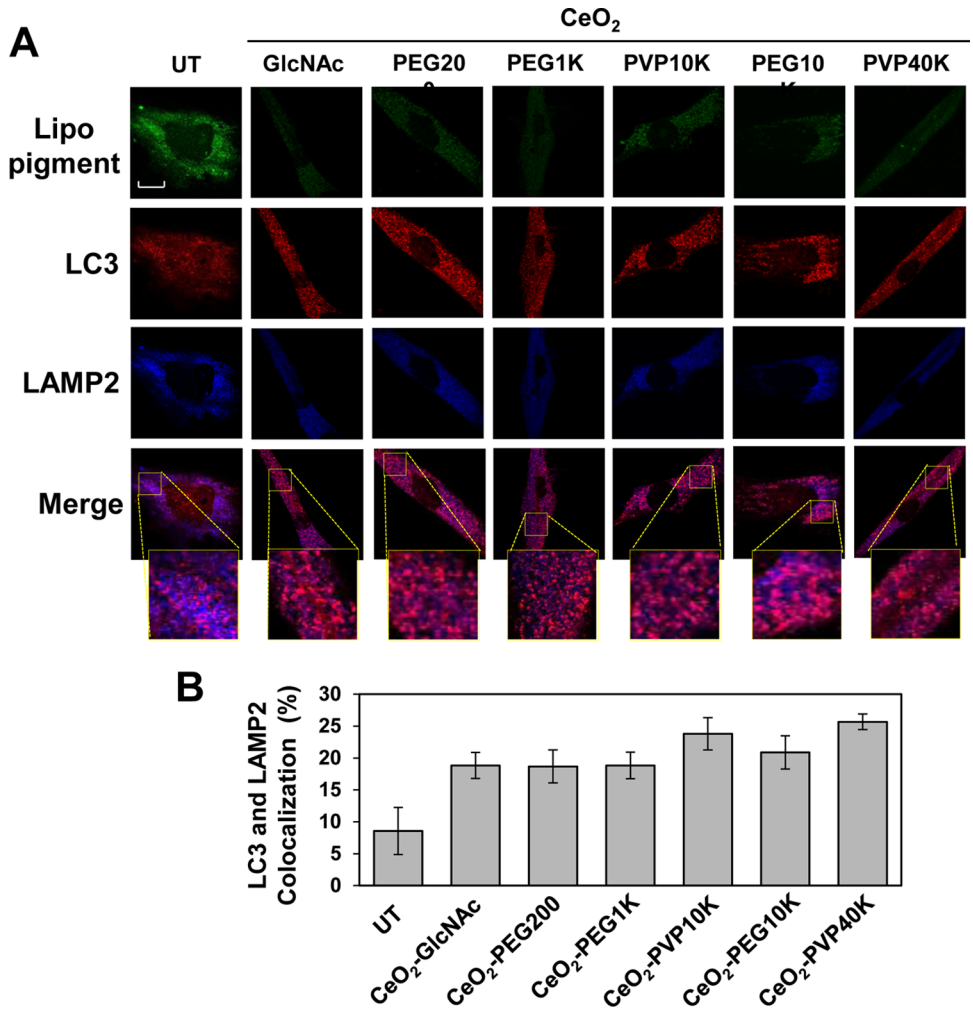

Figure 5. Ceria nanoparticles induced clearance of ceroid lipopigment parallels activation of autophagy in LINCL fibroblasts. (A) Confocal microscopy analyses of ceroid lipopigment (green), LC3 (red), and LAMP-2 (blue) in LINCL fibroblasts treated with 100 ppm of CeO_2 nanoparticles for 3 days, evaluated by detecting green autofluorescence, binding of anti-LC3 antibody, and binding of anti-LAMP-2 antibody, respectively. Colocalization of LC3 and LAMP-2 is shown in merged images (purple). UT, untreated. (B) Quantification of LC3-LAMP-2 colocalization. Data are reported as mean ± SD ($n = 15$; $p < 0.01$). UT, untreated.

exposed to nanoparticles was quantified as described in the Methods and average values, which were calculated over multiple images from replicate samples, were normalized to those obtained from untreated cells (Figure 4B). The fluorescence intensity of ceroid lipopigment in LINCL fibroblasts decreased to approximately 50−60% of that of untreated cells after treatment with CeO_2 nanoparticles (CeO_2−GlcNAc: 51.2 ± 11.5%; CeO_2−PEG200:63.2 ± 10.2%; CeO_2−PEG1K: 59.6 ± 12.9%; CeO_2−PVP10K: 66.0 ± 10.9%; CeO_2−PEG10K: 68.0 ± 11.9%; CeO_2−PVP40K: 64.5 ± 13.1%; Figure 4B; $p < 0.01$), indicating that cell treatment with CeO_2 nanoparticles promotes clearance of ceroid lipopigment.

To confirm that treatment of LINCL cells with CeO_2 nanoparticles, under conditions that result in clearance of ceroid lipopigment, induce TFEB activation, we also evaluated TFEB subcellular localization. Partial nuclear localization of TFEB was observed in untreated LINCL fibroblasts likely due to lipopigment-induced lysosomal stress.[50] Administration of CeO_2 nanoparticles resulted in an increase of TFEB nuclear localization in LINCL fibroblasts (Figure 4A, red), confirming that CeO_2-induced clearance of ceroid lipopigment parallels activation of TFEB.

To confirm that nanoceria-induced nuclear translocation of TFEB in LINCL fibroblasts results in upregulation of genes involved in lysosomal biogenesis and function, we tested the expression of representative genes of the CLEAR network in LINCL cells treated with CeO_2 nanoparticles (100 ppm; 72 h), as described above. We found CeO_2 nanoparticle treatment to cause significant upregulation of *GBA* (from 1.5- to 2.8-fold), *HEXA* (from 1.5- to 2.7-fold), and *LAMP1* (from 1.5- to 2.7-fold) (Figure 4C; $p < 0.05$). To test whether the autophagy system was also transcriptionally activated, we measured the expression of genes of the autophagic pathway. We detected significant upregulation of *MAPLC3* (from 2.7- to 4.4-fold), *SQSTM1* (from 1.8- to 2.9-fold), and *BECN1* (from 2.2- to 3.7-fold)

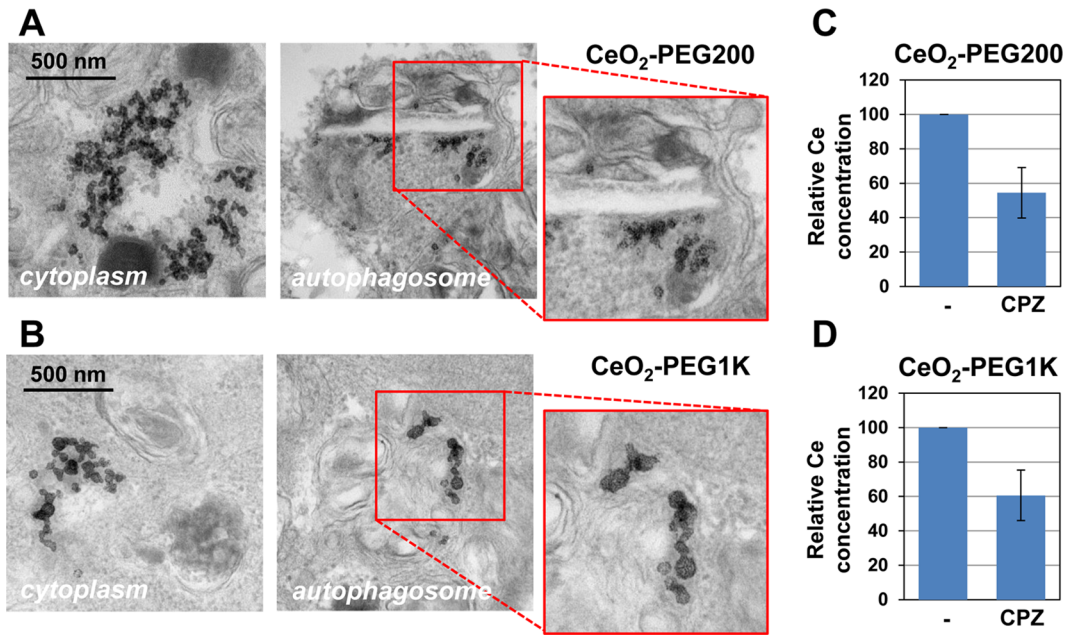

Figure 6. Ceria nanoparticles localize in the cytoplasm and in autophagic vesicles in LINCL cells. TEM analyses of LINCL fibroblasts treated with (A) CeO_2−PEG200 and (B) CeO_2−PEG1K. Representative images of nanoparticles accumulation in the cytoplasm (left) and in autophagic vesicles (right). Scale bar is 500 nm. Cellular uptake of (C) CeO_2−PEG200 and (D) CeO_2−PEG1K upon treatment with chlorpromazine (20 μM) in LINCL cells quantified by ICP-MS. CPZ, chlorpromazine.

(Figure 4D; $p < 0.05$). Taken together, these results demonstrate that TFEB activation and upregulation of genes of the lysosome-autophagy system parallels the reduced accumulation of ceroid lipopigment in cells exposed to CeO_2 nanoparticles.

To confirm enhancement of autophagic flux in cells presenting reduced accumulation of ceroid lipopigment, we tested the extent to which cell treatment with CeO_2 nanoparticles results in autophagosome-lysosome fusion and formation of autophagolysosomes, which is necessary for clearance of cargo.[40] To this end, we evaluated the colocalization of LC3, a protein that is found on the membrane of autophagosomes,[89] with LAMP-2, a protein that resides on the membrane of lysosomes.[90] LINCL fibroblasts were treated with the library of CeO_2 nanoparticles (100 ppm; 3 days). Accumulation of ceroid lipopigment was also monitored by detecting cell autofluorescence (Figure 5A, green). Colocalization of LC3 (red) and LAMP-2 (blue) is shown in merged images (purple). Treatment with CeO_2 nanoparticles resulted in enhanced formation of autophagosomes as indicated by the appearance of punctate LC3 structures. Colocalization of LC3 and LAMP-2 was quantified as described in the Methods and average values were calculated over multiple images and replicate samples (Figure 5B). We observed up to 3-fold increase in the extent of colocalization of LC3 and LAMP-2 in LINCL fibroblasts treated with CeO_2 nanoparticles compared to untreated cells (untreated: 8.6 ± 3.7%; CeO_2−GlcNAc: 18.8 ± 2.0%, CeO_2−PEG200:18.7 ± 2.6%; CeO_2−PEG1K: 18.8 ± 2.1%; CeO_2−PVP10K: 23.8 ± 2.5%; CeO_2−PEG10K: 20.9 ± 2.6%; CeO_2−PVP40K: 25.7 ± 1.2%) (Figure 5B; $p < 0.01$), confirming that CeO_2 nanoparticles promote fusion of autophagosomes and lysosomes and formation of autophagolysosomes.

Intracellular localization of CeO_2 nanoparticles in LINCL fibroblasts was verified by TEM analyses of representative CeO_2 nanoparticles used in this study (CeO_2−PEG200 and CeO_2−PEG1K). TEM images revealed that the CeO_2 nanoparticles localize either in the cytoplasm or in autophagic vesicles in LINCL fibroblasts (Figure 6A,B and Figure S4). Ceria nanoparticles appeared to form aggregates both in the cytoplasm and in autophagic vesicles, most likely due to the high ionic strength conditions of the intracellular environment, which is conducive to nanoparticle aggregation.[91,92] To investigate whether internalization of these CeO_2 nanoparticles occurs *via* endocytosis, we evaluated the intracellular concentration of CeO_2 nanoparticles upon cell treatment with the clathrin-mediated endocytosis inhibitor chlorpromazine. Cells were treated with chlorpromazine at concentrations (20 μM) that result in partial inhibition of endocytosis[93] and do not induce cytotoxicity or affect membrane integrity, thus allowing establishing a correlation between endocytosis and nanoparticle internalization. We found the intracellular concentrations of CeO_2−PEG200 and CeO_2−PEG1K nanoparticles upon treatment with chlorpromazine to decrease to 54.5 ± 14.7% and 60.6 ± 14.6% of the intracellular concentration of CeO_2−PEG200 and CeO_2−PEG1K nanoparticles in untreated cells (Figure 6C,D). While the intracellular fate of CeO_2 nanoparticles remains to

be determined and, particularly, whether cytoplasmic localization occurs upon endosomal escape and whether it precedes autophagosome localization, evidence of CeO_2—PEG200 and CeO_2—PEG1K sequestration in double membrane autophagic vesicles (Figure 6A,B) confirms the interaction of nanoceria with the autophagy system.

In summary, these results demonstrate that cell exposure to CeO_2 nanoparticles induces upregulation of the autophagy system, enhances autophagic activity, and promotes clearance of the autophagic substrate ceroid lipopigment in a model of neuronal ceroid lipofuscinosis.

CONCLUSIONS

Because of their unique properties, nanomaterials interact with biological components and systems, many of which also operate at the nanoscale level. Not surprisingly, nanoparticles of different material, size, and composition were observed to activate autophagy, the main catabolic pathway that is activated to degrade foreign or toxic materials, such as viruses and pathogens.[94,95] We speculated that when nanoparticles are internalized into cells, like any type of nanosized material perceived by the cell as foreign or toxic, they may stimulate the reaction of cellular clearance mechanisms. In this study, we investigated the response of the lysosome-autophagy system to exposure to ceria nanoparticles. We report herein that ceria nanoparticles activate TFEB, a master regulator of lysosomal biogenesis and autophagy, thereby inducing upregulation of the pathway at the transcriptional level. We found that CeO_2 nanoparticles activate autophagy without inducing cytotoxicity or apoptosis and promote clearance of toxic aggregates in disease cells that have an inefficient lysosomal system.

Recent studies suggest that lysosomal impairment may be associated with the mechanism of nanoparticle-induced cytotoxicity. Nanoparticles presenting cationic surfaces were specifically reported to disrupt lysosomes by inducing a "proton sponge" effect.[65] Unlike other types of nanomaterials that once internalized by cells induce enhanced formation of autophagosomes, but also impair lysosome function, thereby disrupting the autophagic flux,[42,96,97] CeO_2 nanoparticles do not impair lysosomes, but promote clearance, thus ultimately resulting in enhanced degradation of autophagic cargo. This study provides a mechanistic understanding of the interaction of ceria nanoparticles with this important cellular catabolic pathway, thus furthering our understanding of the environmental impact of ceria nanoparticles and laying the foundation for the design of nanotherapeutics for the treatment of diseases characterized by inefficient autophagic activity and accumulation of storage material.

The fate of the ceria nanoparticles upon activation of the autophagy system and upregulation of autophagic clearance remains to be determined. *In vitro* studies revealed that metal nanoparticles including gold, superparamagnetic iron oxide, and quantum dots, are removed from cells through exocytosis.[98,99] Exocytosis of autolysosomes was previously reported as a mechanism of TFEB-mediated clearance[71] and it is thus likely to be induced by nanoparticle autophagy activators, such as the six differently surface functionalized CeO_2 nanoparticles analyzed in this study.

Inefficient autophagic clearance underlies the development and progression of a number of human diseases, ranging from neurodegenerative diseases to cancer. For instance, affected cells from patients with lysosomal storage disorders present accumulation of proteolipid and glycoprotein substrates.[100] Among lysosomal storage disorders, NCLs are the most devastating inherited disorders of childhood and the most common cause of neurodegeneration in children in the US. In this study, we demonstrated that nanoceria promotes clearance of ceroid lipopigment deposits in cells derived from a patient affected by LINCL, which is characterized by a defective lysosome-autophagy system. While it remains to be demonstrated whether CeO_2 nanoparticles enhance clearance of other autophagic cargos, results from this study provide proof of principle evidence of the use of nanomaterials as a platform for the development of nanotherapeutics that enhance TFEB-mediated activation of autophagy, with tremendous implications for the treatment of diseases characterized by storage of autophagic substrates.

METHODS

Reagents and Cell Cultures. Cerium nitrate hexahydrate ($Ce(NO_3)_3 \cdot 6H_2O$), oleylamine, 1-octadecene, *N*-acetyl-D-glucosamine (GlcNAc), Polyethylene glycol (PEG200, PEG1K, PEG10K), Polyvinylpyrrolidone (PVP10K and PVP40K) were purchased from Sigma-Aldrich. Hexane, acetone, and ethanol were purchased from Fisher Scientific.

Cell culture medium was purchased from Lonza. Chloroquine (CQ) was from Sigma-Aldrich. DQ Green BSA was from Invitrogen.

Fibroblasts derived from patients with late infantile neuronal ceroid lipofuscinosis type 2 (LINCL) were obtained from Coriell Cell Repositories (GM16486). HeLa cells stably transfected for the expression of TFEB-3xFLAG were a generous gift of Dr. Sardiello.[50] Cells were grown at 37 °C in 5% CO_2 in Dulbecco's Modified Eagle Medium, supplemented with heat-inactivated fetal bovine serum (20% FBS for LINCL fibroblasts and 10% FBS for Hela cells) and 1% glutamine Pen-Strep. The medium was replaced every 3 or 4 days and monolayers were passaged with TrypLE Express.

Synthesis of Monodisperse Ceria Nanocrystals. Nanocrystalline cerium oxides were synthesized using the cerium precursor decomposition method at high temperature.[72] Cerium nitrate hexahydrate (10 mmol, 4.34 g) were mixed with oleylamine

(30 mmol, 8.02 g) in 1-octadecene (120 mmol, 30 g) and stirred vigorously at room temperature. The reaction mixture was dissolved in 1-octadecene at 80 °C, forming yellow cerium-oleylamine mixture. This cerium precursor was decomposed at 260 °C and near-spherical ceria nanocrystals with narrow diameter distribution ($\sigma < 10\%$) were prepared after 2 h reaction at 260 °C under ultrahigh purity nitrogen condition. The resulting dark brown ceria nanocrystals were purified by addition of 25 mL of ethanol and precipitated by adding 25 mL of acetone. The precipitates were separated from unreacted cerium precursor, oleylamine, and 1-octadecene by centrifugation at 6000 rpm for 30 min. The purification process was repeated 3 times and purified ceria nanocrystals were redispersed in hexane.

Phase Transfer of Ceria Nanocrystals. Water-soluble nanocrystals were produced using various phase transfer agents (GlcNAc, PEG200, PEG1K, PEG10K, PVP10K, and PVP40K). Specifically, 1 mL of ceria nanocrystal/hexane solution ([Ce] = 6820 mg/L) was mixed with the phase transfer agent (GlcNAc (1.8 mg), PEG200 (1.2 mg), PEG1K (1.0 mg), PEG10K (1.0 mg), PVP10K (0.05 mg), or PVP40K (0.08 mg)) in 15 mL of ultrapure water (Millipore, 18.2 MΩ·cm). This suspension was then sonicated using a probe-sonicator (Hielscher UP50H) for 20 min at 80% amplitude and full cycle. The phase transferred nanocrystals were purified by ultracentrifugation at 45 000 rpm for 4 h and by membrane filtration (Ultrafiltration cellulose membranes, 30 kDa MWCO) using a stirred Cell (Amicon) to remove the excess of free phase transfer agents left in the supernatant. The purification was repeated 3 times and phase transferred ceria nanocrystals were stored in ultrapure water.

Characterization of Ceria Nanocrystals. TEM specimens were prepared by dropping the nanocrystal solution on ultrathin carbon type A 400 mesh copper grids (Ted Pella Inc.). The TEM micrographs were taken on a JEOL 2100 field emission gun TEM operated at 200 kV with a single tilt holder. Inductively coupled plasma atomic emission spectroscopy (ICP-AES) was used to measure the concentration of ceria nanocrystals. ICP-AES analysis was carried out using a PerkinElmer ICP-AES instrument equipped with autosampler. Hydrodynamic radius and surface charge of water-soluble ceria nanocrystals were analyzed at 25 °C using DLS and zeta potential using a Malvern Nano ZS system by Malvern Instruments (Malvern Zetasizer Nanoseries, Malvern, UK).

Cellular Uptake of Ceria Nanocrystals. 10^5 cells were plated in each well of 6-well plates and incubated overnight to allow cell attachment. Ceria nanoparticles were diluted in complete medium and added to cell cultures to a final concentration of 100 ppm. Cells were exposed to ceria nanoparticles for 24 h, washed with PBS and incubated with acidic solution (50 mM glycine, 100 mM sodium chloride, 2 mg/mL polyvinylpyrrolidone (MW: 40K), pH 3) to remove membrane-binding nanocrystals as previously described.[101] After acid strip, cells were washed with DI water, collected and digested with 1% HNO_3. The amount of ceria nanoparticles internalized by the cells was quantified using inductively coupled plasma mass spectrometry (ICP-MS; PerkinElmer ELAN9000): the concentration of cerium atoms in each well was measured, and the number of ceria nanoparticles was calculated on the basis of the number of atoms in each particle as previously described.[72]

To prepare TEM samples, LINCL fibroblasts were seeded in 6 well plates to 70−80% confluence, cultured in the presence of ceria nanoparticles for 24 h, washed with PBS and fixed with 2% paraformaldehyde and 3% glutaraldehyde in 0.1 M PBS. After fixation, the samples were washed in 0.1 M cacodylate buffer and treated with 0.1% Millipore-filtered buffered tannic acid, postfixed with 1% buffered osmium tetroxide for 30 min, and stained en bloc with 1% Millipore-filtered uranyl acetate. The samples were washed several times in water, then dehydrated in increasing concentrations of ethanol, infiltrated, and embedded in LX-112 medium. The samples were polymerized in a 60 °C oven for 2 days. Ultrathin sections were cut in a Leica Ultracut microtome (Leica, Deerfield, IL), stained with uranyl acetate and lead citrate in a Leica EM Stainer, and examined in a JEM 1010 transmission electron microscope (JEOL, USA, Inc., Peabody, MA) at an accelerating voltage of 80 kV. Digital images were obtained using AMT Imaging System (Advanced Microscopy Techniques Corp, Danvers, MA).

Immunofluorescence Assays. Cells were seeded on glass coverslips, cultured in the presence of ceria nanoparticles as indicated in each experiment, and fixed with 4% paraformaldehyde for 30 min. Cells were then permeabilized with 0.1% Triton-X for 5 min and incubated with 8% BSA for 1 h. Following incubation for 1 h with primary antibodies (rabbit anti-FLAG (Sigma-Aldrich; 1:1000), mouse anti-TFEB (Abcam; 1:100), rabbit anti-LC3 (MBL; 1:2000), or mouse anti-LAMP2 (Biolegend; 1:2000) antibodies), cells were washed three times with 0.1% Tween-20/PBS, and then incubated with secondary antibodies for 1 h (Dylight 549 goat antirabbit (KPL, 1:500) and Dylight 649 goat antimouse (KPL, 1:500) antibodies. Images were obtained using an Olympus IX81 confocal microscope and colocalized using the Fluoview software. Images were quantitatively analyzed using NIH ImageJ analysis software and MATLAB.

Quantitative RT-PCR. Quantitative RT-PCR was performed as previously described.[102] Cells were incubated with ceria nanoparticles for indicated time lengths before total RNA was extracted using $_{RNA}$GEM reagent (ZyGEM). cDNA was synthesized from total RNA using qScript cDNA SuperMix (Quanta Biosciences). Total cDNA amount was measured by NanoDrop 2000 (Thermo Scientific). qRT-PCR reactions were performed using cDNA, PerfeCTa SYBR Green FastMix (Quanta Biosciences) and corresponding primers (Table S1) in the CFX96 Real-Time PCR detection system (Bio-Rad). Samples were heated for 2 min at 95 °C and amplified in 45 cycles of 1 s at 95 °C, 30 s at 60 °C, and 30 s at 72 °C. Analyses were conducted using CFX manager software (Bio-Rad) and the threshold cycle (C_T) was extracted from the PCR amplification plot. The ΔC_T value was calculated as previously described[103] to normalize the C_T of each target gene to that of the housekeeping genes *GAPDH* and *ACTB*. The relative mRNA expression level of each target gene in treated cells was normalized to that measured in untreated cells: relative mRNA expression level = $2^{[-(\Delta C_T \text{ (treated cells)} - \Delta C_T \text{ (untreated cells)})]}$. Each data point was evaluated in triplicate and measured three times.

Apoptosis Assays. Apoptosis assay was conducted as previously described.[104] Briefly, cells were collected after 24 h of incubation with ceria nanoparticles. Cell toxicity was tested using the CytoGLO Annexin V-FITC Apoptosis Detection Kit (IMGENEX) according to the manufacturer's instructions and analyzed by flow cytometry (FACSCanto II, Beckon Dickingson) with a 488 nm Argon laser.

Cell Viability Assays. Cell viability assay was performed using LIVE/DEAD Viability/Cytotoxicity Kit (Molecular Probes). Cells were seeded on glass coverslips and cultured in the presence of ceria nanoparticles for 24 h. Cells were washed twice with PBS, and then incubated with 2 μM calcein AM and 4 μM ethidium homodimer (EthD-1) reagents according to the manufacturer's instructions. Images were obtained using an Olympus IX81 confocal microscope and colocalized using the Fluoview software.

DQ-BSA Assays. DQ-BSA assay was conducted as previously described.[42] Cells were incubated with ceria nanoparticles for 24 h, washed with PBS, and then incubated in DMEM medium containing 10 μg/mL DQ Green BSA (Molecular Probes) for 3 h at 37 °C. Cells were then washed again with PBS and analyzed by flow cytometry (FACSCanto II, Beckon Dickingson) with a 488 nm Argon laser.

Western Blot Analyses. Cells were incubated with ceria nanoparticles for 24 h, collected and lysed with the complete lysis-M buffer containing the protease inhibitor cocktail (Roche). Total protein concentrations were determined by Bradford assay (Thermo Scientific) and each sample was diluted to the same protein concentration. Aliquots of cell lysates were separated by 15% SDS-PAGE gel. Western blot analyses were performed using primary antibodies (rabbit anti-LC3 (MBL), or rabbit anti-GAPDH (Santa Cruz Biotechnology) antibodies) and HRP-conjugated goat antirabbit (Santa Cruz Biotechnology) as the secondary antibody. Blots were visualized using Luminata Forte Western HRP substrate (Millipore).

Quantification of Immunofluorescence Images. The accumulation of ceroid lipopigment was quantified as previously described by

measuring the brightness density of each image and calculating the ratio of brightness density of CeO_2 nanoparticle treated cells over that of untreated cells.[76] Average values were taken over multiple images from replicate samples.

Colocalization of LC3 and LAMP-2 was quantified by calculating the number of pixels presenting brightness (0−255 gray scale) of red and blue above a predefined threshold (gray scale >30) and with ratio of red to blue within a predefined range (0.5−2). The percentage of colocalization was calculated by normalizing the number of pixels presenting LC3 and LAMP-2 colocalization by the total number of pixels presenting either LC3 or LAMP-2 signal in each cell over the entire image. Average values were calculated over multiple images and replicate samples.

Statistical Analyses. All data is presented as mean ± SD, and statistical significance was calculated using a two-tailed *t*-test.

Conflict of Interest: The authors declare no competing financial interest.

Acknowledgment. This work was funded by The National Science Foundation (CBET-1336053 and CBET 1254318) and the Welch Foundation (C-1824). TEM analyses were conducted by the UT MD Anderson Cancer Center High Resolution Electron Microscopy Facility (Institutional Core Grant #CA16672).

Supporting Information Available: Primer sequences used in quantitative RT-PCR, TFEB activation in HeLa/TFEB cells exposed to 2-hydroxypropyl-β-cyclodextrin, apoptosis induction in HeLa/TFEB cells after prolonged exposure to ceria nanoparticles, cytotoxicity assay in nanoceria treated HeLa/TFEB cells, TEM analysis of untreated LINCL fibroblasts. This material is available free of charge *via* the Internet at http://pubs.acs.org.

REFERENCES AND NOTES

1. Tsunekawa, S.; Fukuda, T.; Kasuya, A. Blue Shift in Ultraviolet Absorption Spectra of Monodisperse CeO_{2-X} Nanoparticles. *J. Appl. Phys.* **2000**, *87*, 1318–1321.
2. Fu, Q.; Saltsburg, H.; Flytzani-Stephanopoulos, M. Active Nonmetallic Au and Pt Species on Ceria-Based Water-Gas Shift Catalysts. *Science* **2003**, *301*, 935–938.
3. Tabakova, T.; Boccuzzi, F.; Manzoli, M.; Sobczak, J. W.; Idakiev, V.; Andreeva, D. A Comparative Study of Nanosized IB/Ceria Catalysts for Low-Temperature Water-Gas Shift Reaction. *Appl. Catal., A* **2006**, *298*, 127–143.
4. Trovarelli, A. Catalytic Properties of Ceria and CeO_2-Containing Materials. *Catal. Rev. Sci. Eng.* **1996**, *38*, 439–520.
5. Esch, F.; Fabris, S.; Zhou, L.; Montini, T.; Africh, C.; Fornasiero, P.; Comelli, G.; Rosei, R. Electron Localization Determines Defect Formation on Ceria Substrates. *Science* **2005**, *309*, 752–755.
6. Liu, X.; Zhou, K.; Wang, L.; Wang, B.; Li, Y. Oxygen Vacancy Clusters Promoting Reducibility and Activity of Ceria Nanorods. *J. Am. Chem. Soc.* **2009**, *131*, 3140–3141.
7. Bunluesin, T.; Gorte, R. J.; Graham, G. W. Studies of the Water-Gas-Shift Reaction on Ceria-Supported Pt, Pd, and Rh: Implications for Oxygen-Storage Properties. *Appl. Catal., B* **1998**, *15*, 107–114.
8. Wheeler, C.; Jhalani, A.; Klein, E. J.; Tummala, S.; Schmidt, L. D. The Water-Gas-Shift Reaction at Short Contact Times. *J. Catal.* **2004**, *223*, 191–199.
9. Deluga, G. A.; Salge, J. R.; Schmidt, L. D.; Verykios, X. E. Renewable Hydrogen from Ethanol by Autothermal Reforming. *Science* **2004**, *303*, 993–997.
10. Farrauto, R.; Hwang, S.; Shore, L.; Ruettinger, W.; Lampert, J.; Giroux, T.; Liu, Y.; Ilinich, O. New Material Needs for Hydrocarbon Fuel Processing: Generating Hydrogen for the PEM Fuel Cell. *Annu. Rev. Mater. Res.* **2003**, *33*, 1–27.
11. Uchiyama, T.; Yoshida, H.; Kuwauchi, Y.; Ichikawa, S.; Shimada, S.; Haruta, M.; Takeda, S. Systematic Morphology Changes of Gold Nanoparticles Supported on CeO_2 During CO Oxidation. *Angew. Chem., Int. Ed. Engl.* **2011**, *50*, 10157–10160.
12. Health Effects Institute. *Evaluation of Human Health Risk from Cerium Added to Diesel Fuel*. Communication 9, **2011**.
13. Jung, H.; Kittelson, D. B.; Zachariah, M. R. The Influence of a Cerium Additive on Ultrafine Diesel Particle Emissions and Kinetics of Oxidation. *Combust. Flame* **2005**, *142*, 276–288.
14. Sajeevan, A. C.; Sajith, V. Diesel Engine Emission Reduction Using Catalytic Nanoparticles: An Experimental Investigation. *J. Eng.* **2013**, 10.1155/2013/589382.
15. Batley, G. E.; Halliburton, B.; Kirby, J. K.; Doolette, C. L.; Navarro, D.; McLaughlin, M. J.; Veitch, C. Characterization and Ecological Risk Assessment of Nanoparticulate CeO_2 as a Diesel Fuel Catalyst. *Environ. Toxicol. Chem.* **2013**, *32*, 1896–1905.
16. Cassee, F. R.; van Balen, E. C.; Singh, C.; Green, D.; Muijser, H.; Weinstein, J.; Dreher, K. Exposure, Health and Ecological Effects Review of Engineered Nanoscale Cerium and Cerium Oxide Associated with Its Use as a Fuel Additive. *Crit. Rev. Toxicol.* **2011**, *41*, 213–229.
17. Steiner, S.; Mueller, L.; Popovicheva, O. B.; Raemy, D. O.; Czerwinski, J.; Comte, P.; Mayer, A.; Gehr, P.; Rothen-Rutishauser, B.; Clift, M. J. Cerium Dioxide Nanoparticles Can Interfere with the Associated Cellular Mechanistic Response to Diesel Exhaust Exposure. *Toxicol. Lett.* **2012**, *214*, 218–225.
18. Hardas, S. S.; Sultana, R.; Warrier, G.; Dan, M.; Wu, P.; Grulke, E. A.; Tseng, M. T.; Unrine, J. M.; Graham, U. M.; Yokel, R. A.; Butterfield, D. A. Rat Hippocampal Responses up to 90 Days after a Single Nanoceria Dose Extends a Hierarchical Oxidative Stress Model for Nanoparticle Toxicity. *Nanotoxicology* **2014**, *8*, 155–166.
19. Karakoti, A. S.; Monteiro-Riviere, N. A.; Aggarwal, R.; Davis, J. P.; Narayan, R. J.; Self, W. T.; McGinnis, J.; Seal, S. Nanoceria as Antioxidant: Synthesis and Biomedical Applications. *JOM* **2008**, No. 60, 33–37.
20. Schubert, D.; Dargusch, R.; Raitano, J.; Chan, S. W. Cerium and Yttrium Oxide Nanoparticles Are Neuroprotective. *Biochem. Biophys. Res. Commun.* **2006**, *342*, 86–91.
21. Lee, S. S.; Song, W.; Cho, M.; Puppala, H. L.; Nguyen, P.; Zhu, H.; Segatori, L.; Colvin, V. L. Antioxidant Properties of Cerium Oxide Nanocrystals as a Function of Nanocrystal Diameter and Surface Coating. *ACS Nano* **2013**, *7*, 9693–9703.
22. Xia, T.; Kovochich, M.; Liong, M.; Madler, L.; Gilbert, B.; Shi, H.; Yeh, J. I.; Zink, J. I.; Nel, A. E. Comparison of the Mechanism of Toxicity of Zinc Oxide and Cerium Oxide Nanoparticles Based on Dissolution and Oxidative Stress Properties. *ACS Nano* **2008**, *2*, 2121–2134.
23. Korsvik, C.; Patil, S.; Seal, S.; Self, W. T. Superoxide Dismutase Mimetic Properties Exhibited by Vacancy Engineered Ceria Nanoparticles. *Chem. Commun.* **2007**, 1056–1058.
24. Das, M.; Patil, S.; Bhargava, N.; Kang, J. F.; Riedel, L. M.; Seal, S.; Hickman, J. J. Auto-Catalytic Ceria Nanoparticles Offer Neuroprotection to Adult Rat Spinal Cord Neurons. *Biomaterials* **2007**, *28*, 1918–1925.
25. Colon, J.; Hsieh, N.; Ferguson, A.; Kupelian, P.; Seal, S.; Jenkins, D. W.; Baker, C. H. Cerium Oxide Nanoparticles Protect Gastrointestinal Epithelium from Radiation-Induced Damage by Reduction of Reactive Oxygen Species and Upregulation of Superoxide Dismutase 2. *Nanomedicine* **2010**, *6*, 698–705.
26. Tarnuzzer, R. W.; Colon, J.; Patil, S.; Seal, S. Vacancy Engineered Ceria Nanostructures for Protection from Radiation-Induced Cellular Damage. *Nano Lett.* **2005**, *5*, 2573–2577.
27. Chen, J.; Patil, S.; Seal, S.; McGinnis, J. F. Rare Earth Nanoparticles Prevent Retinal Degeneration Induced by Intracellular Peroxides. *Nat. Nanotechnol.* **2006**, *1*, 142–150.
28. Chen, J.; Patil, S.; Seal, S.; McGinnis, J. F. Nanoceria Particles Prevent ROI-Induced Blindness. *Adv. Exp. Med. Biol.* **2008**, *613*, 53–59.

29. Lin, W.; Huang, Y. W.; Zhou, X. D.; Ma, Y. Toxicity of Cerium Oxide Nanoparticles in Human Lung Cancer Cells. *Int. J. Toxicol.* **2006**, *25*, 451–457.
30. Hussain, S.; Al-Nsour, F.; Rice, A. B.; Marshburn, J.; Yingling, B.; Ji, Z.; Zink, J. I.; Walker, N. J.; Garantziotis, S. Cerium Dioxide Nanoparticles Induce Apoptosis and Autophagy in Human Peripheral Blood Monocytes. *ACS Nano* **2012**, *6*, 5820–5829.
31. Hussain, S.; Garantziotis, S. Interplay between Apoptotic and Autophagy Pathways after Exposure to Cerium Dioxide Nanoparticles in Human Monocytes. *Autophagy* **2013**, *9*, 101–103.
32. Graham, U. M.; Tseng, M. T.; Jasinski, J. B.; Yokel, R. A.; Unrine, J. M.; Davis, B. H.; Dozier, A. K.; Hardas, S. S.; Sultana, R.; Grulke, E. A.; Butterfield, D. A. *In Vivo* Processing of Ceria Nanoparticles inside Liver: Impact on Free-Radical Scavenging Activity and Oxidative Stress. *ChemPlusChem* **2014**, *79*, 1083–1088.
33. Lee, C. M.; Huang, S. T.; Huang, S. H.; Lin, H. W.; Tsai, H. P.; Wu, J. Y.; Lin, C. M.; Chen, C. T. C60 Fullerene-Pentoxifylline Dyad Nanoparticles Enhance Autophagy to Avoid Cytotoxic Effects Caused by the Beta-Amyloid Peptide. *Nanomedicine* **2011**, *7*, 107–114.
34. Li, H.; Li, Y.; Jiao, J.; Hu, H. M. Alpha-Alumina Nanoparticles Induce Efficient Autophagy-Dependent Cross-Presentation and Potent Antitumour Response. *Nat. Nanotechnol.* **2011**, *6*, 645–650.
35. Li, J. J.; Hartono, D.; Ong, C. N.; Bay, B. H.; Yung, L. Y. Autophagy and Oxidative Stress Associated with Gold Nanoparticles. *Biomaterials* **2010**, *31*, 5996–6003.
36. Seleverstov, O.; Zabirnyk, O.; Zscharnack, M.; Bulavina, L.; Nowicki, M.; Heinrich, J. M.; Yezhelyev, M.; Emmrich, F.; O'Regan, R.; Bader, A. Quantum Dots for Human Mesenchymal Stem Cells Labeling. A Size-Dependent Autophagy Activation. *Nano Lett.* **2006**, *6*, 2826–2832.
37. Yokoyama, T.; Tam, J.; Kuroda, S.; Scott, A. W.; Aaron, J.; Larson, T.; Shanker, M.; Correa, A. M.; Kondo, S.; Roth, J. A.; *et al.* EGFR-Targeted Hybrid Plasmonic Magnetic Nanoparticles Synergistically Induce Autophagy and Apoptosis in Non-Small Cell Lung Cancer Cells. *PLoS One* **2011**, *6*, e25507.
38. Zhang, Q.; Yang, W.; Man, N.; Zheng, F.; Shen, Y.; Sun, K.; Li, Y.; Wen, L. P. Autophagy-Mediated Chemosensitization in Cancer Cells by Fullerene C60 Nanocrystal. *Autophagy* **2009**, *5*, 1107–1117.
39. Yu, L.; Lu, Y.; Man, N.; Yu, S. H.; Wen, L. P. Rare Earth Oxide Nanocrystals Induce Autophagy in Hela Cells. *Small* **2009**, *5*, 2784–2787.
40. Klionsky, D. J. Autophagy: From Phenomenology to Molecular Understanding in Less Than a Decade. *Nat. Rev. Mol. Cell Biol.* **2007**, *8*, 931–937.
41. Zhang, Y.; Zheng, F.; Yang, T.; Zhou, W.; Liu, Y.; Man, N.; Zhang, L.; Jin, N.; Dou, Q.; Zhang, Y.; Li, Z.; Wen, L.-P. Tuning the Autophagy-Inducing Activity of Lanthanide-Based Nanocrystals through Specific Surface-Coating Peptides. *Nat. Mater.* **2012**, *11*, 817–826.
42. Ma, X.; Wu, Y.; Jin, S.; Tian, Y.; Zhang, X.; Zhao, Y.; Yu, L.; Liang, X. J. Gold Nanoparticles Induce Autophagosome Accumulation through Size-Dependent Nanoparticle Uptake and Lysosome Impairment. *ACS Nano* **2011**, *5*, 8629–8639.
43. Kroemer, G.; Levine, B. Autophagic Cell Death: The Story of a Misnomer. *Nat. Rev. Mol. Cell Biol.* **2008**, *9*, 1004–1010.
44. Debnath, J.; Baehrecke, E. H.; Kroemer, G. Does Autophagy Contribute to Cell Death? *Autophagy* **2005**, *1*, 66–74.
45. Eisenberg-Lerner, A.; Bialik, S.; Simon, H. U.; Kimchi, A. Life and Death Partners: Apoptosis, Autophagy and the Cross-Talk between Them. *Cell Death Differ.* **2009**, *16*, 966–975.
46. Roy, R.; Singh, S. K.; Chauhan, L. K.; Das, M.; Tripathi, A.; Dwivedi, P. D. Zinc Oxide Nanoparticles Induce Apoptosis by Enhancement of Autophagy *via* PI3K/Akt/mTOR Inhibition. *Toxicol. Lett.* **2014**, *227*, 29–40.
47. Afeseh Ngwa, H.; Kanthasamy, A.; Gu, Y.; Fang, N.; Anantharam, V.; Kanthasamy, A. G. Manganese Nanoparticle Activates Mitochondrial Dependent Apoptotic Signaling and Autophagy in Dopaminergic Neuronal Cells. *Toxicol. Appl. Pharmacol.* **2011**, *256*, 227–240.
48. Horie, M.; Nishio, K.; Kato, H.; Fujita, K.; Endoh, S.; Nakamura, A.; Miyauchi, A.; Kinugasa, S.; Yamamoto, K.; Niki, E.; *et al.* Cellular Responses Induced by Cerium Oxide Nanoparticles: Induction of Intracellular Calcium Level and Oxidative Stress on Culture Cells. *J. Biochem.* **2011**, *150*, 461–471.
49. Ma, J. Y.; Zhao, H.; Mercer, R. R.; Barger, M.; Rao, M.; Meighan, T.; Schwegler-Berry, D.; Castranova, V.; Ma, J. K. Cerium Oxide Nanoparticle-Induced Pulmonary Inflammation and Alveolar Macrophage Functional Change in Rats. *Nanotoxicology* **2011**, *5*, 312–325.
50. Sardiello, M.; Palmieri, M.; di Ronza, A.; Medina, D. L.; Valenza, M.; Gennarino, V. A.; Di Malta, C.; Donaudy, F.; Embrione, V.; Polishchuk, R. S.; *et al.* A Gene Network Regulating Lysosomal Biogenesis and Function. *Science* **2009**, *325*, 473–477.
51. Palmieri, M.; Impey, S.; Kang, H.; di Ronza, A.; Pelz, C.; Sardiello, M.; Ballabio, A. Characterization of the Clear Network Reveals an Integrated Control of Cellular Clearance Pathways. *Hum. Mol. Genet.* **2011**, *20*, 3852–3866.
52. Song, W.; Wang, F.; Savini, M.; Ake, A.; di Ronza, A.; Sardiello, M.; Segatori, L. TFEB Regulates Lysosomal Proteostasis. *Hum. Mol. Genet.* **2013**, *22*, 1994–2009.
53. Settembre, C.; Di Malta, C.; Polito, V. A.; Garcia Arencibia, M.; Vetrini, F.; Erdin, S.; Erdin, S. U.; Huynh, T.; Medina, D.; Colella, P.; *et al.* TFEB Links Autophagy to Lysosomal Biogenesis. *Science* **2011**, *332*, 1429–1433.
54. Sardiello, M.; Ballabio, A. Lysosomal Enhancement: A Clear Answer to Cellular Degradative Needs. *Cell Cycle* **2009**, *8*, 4021–4022.
55. Settembre, C.; Ballabio, A. TFEB Regulates Autophagy: An Integrated Coordination of Cellular Degradation and Recycling Processes. *Autophagy* **2011**, *7*, 1379–1381.
56. Gray, W. D.; Che, P.; Brown, M.; Ning, X.; Murthy, N.; Davis, M. E. *N*-Acetylglucosamine Conjugated to Nanoparticles Enhances Myocyte Uptake and Improves Delivery of a Small Molecule P38 Inhibitor for Post-Infarct Healing. *J. Cardiovasc. Transl. Res.* **2011**, *4*, 631–643.
57. Levit, R. D.; Taylor, W. R. A Clinical Commentary on the Article "*N*-Acetylglucosamine Conjugated to Nanoparticles Enhances Myocyte Uptake and Improves Delivery of a Small Molecule P38 Inhibitor for Post-Infarct Healing": *N*-Acetylglucosamine Conjugated Nanoparticles: Translational Opportunities and Barriers. *J. Cardiovasc. Transl. Res.* **2011**, *4*, 644–645.
58. Otsuka, H.; Nagasaki, Y.; Kataoka, K. Pegylated Nanoparticles for Biological and Pharmaceutical Applications. *Adv. Drug Delivery Rev.* **2003**, *55*, 403–419.
59. Nance, E. A.; Woodworth, G. F.; Sailor, K. A.; Shih, T. Y.; Xu, Q.; Swaminathan, G.; Xiang, D.; Eberhart, C.; Hanes, J. A Dense Poly(ethylene glycol) Coating Improves Penetration of Large Polymeric Nanoparticles within Brain Tissue. *Sci. Transl. Med.* **2012**, *4*, 149ra119.
60. Gupta, A. K.; Gupta, M. Synthesis and Surface Engineering of Iron Oxide Nanoparticles for Biomedical Applications. *Biomaterials* **2005**, *26*, 3995–4021.
61. Rose, P. A.; Praseetha, P. K.; Bhagat, M.; Alexander, P.; Abdeen, S.; Chavali, M. Drug Embedded PVP Coated Magnetic Nanoparticles for Targeted Killing of Breast Cancer Cells. *Technol. Cancer Res. Treat.* **2013**, *12*, 463–472.
62. Arsalani, N.; Fattahi, H.; Nazarpoor, M. Synthesis and Characterization of PVP-Functionalized Superparamagnetic Fe_3O_4 Nanoparticles as an MRI Contrast Agent. *Express Polym. Lett.* **2010**, *4*, 329–338.
63. Frohlich, E.; Meindl, C.; Roblegg, E.; Ebner, B.; Absenger, M.; Pieber, T. R. Action of Polystyrene Nanoparticles of Different Sizes on Lysosomal Function and Integrity. *Part. Fibre Toxicol.* **2012**, *9*, 26.
64. Stern, S.; Adiseshaiah, P.; Crist, R. Autophagy and Lysosomal Dysfunction as Emerging Mechanisms of Nanomaterial Toxicity. *Part. Fibre Toxicol.* **2012**, *9*, 20.

65. Xia, T.; Kovochich, M.; Liong, M.; Zink, J. I.; Nel, A. E. Cationic Polystyrene Nanosphere Toxicity Depends on Cell-Specific Endocytic and Mitochondrial Injury Pathways. *ACS Nano* **2008**, *2*, 85–96.
66. Settembre, C.; Fraldi, A.; Jahreiss, L.; Spampanato, C.; Venturi, C.; Medina, D.; de Pablo, R.; Tacchetti, C.; Rubinsztein, D. C.; Ballabio, A. A Block of Autophagy in Lysosomal Storage Disorders. *Hum. Mol. Genet.* **2008**, *17*, 119–129.
67. Shimada, Y.; Klionsky, D. J. Autophagy Contributes to Lysosomal Storage Disorders. *Autophagy* **2012**, *8*, 715–716.
68. Pierret, C.; Morrison, J. A.; Kirk, M. D. Treatment of Lysosomal Storage Disorders: Focus on the Neuronal Ceroid-Lipofuscinoses. *Acta Neurobiol. Exp.* **2008**, *68*, 429–442.
69. Williams, R. E.; Mole, S. E. New Nomenclature and Classification Scheme for the Neuronal Ceroid Lipofuscinoses. *Neurology* **2012**, *79*, 183–191.
70. Kohlschutter, A.; Schulz, A. Towards Understanding the Neuronal Ceroid Lipofuscinoses. *Brain Dev.* **2009**, *31*, 499–502.
71. Medina, D. L.; Fraldi, A.; Bouche, V.; Annunziata, F.; Mansueto, G.; Spampanato, C.; Puri, C.; Pignata, A.; Martina, J. A.; Sardiello, M.; *et al.* Transcriptional Activation of Lysosomal Exocytosis Promotes Cellular Clearance. *Dev. Cell* **2011**, *21*, 421–430.
72. Lee, S. S.; Zhu, H.; Contreras, E. Q.; Prakash, A.; Puppala, H. L.; Colvin, V. L. High Temperature Decomposition of Cerium Precursors to Form Ceria Nanocrystal Libraries for Biological Applications. *Chem. Mater.* **2012**, *24*, 424–432.
73. Caschera, D.; Federici, F.; Zane, D.; Focanti, F.; Curulli, A.; Padeletti, G. Gold Nanoparticles Modified GC Electrodes: Electrochemical Behaviour Dependence of Different Neurotransmitters and Molecules of Biological Interest on the Particles Size and Shape. *J. Nanopart. Res.* **2008**, *11*, 1925–1936.
74. Behera, M.; Ram, S. Spectroscopy-Based Study on the Interaction between Gold Nanoparticle and Poly-(vinylpyrrolidone) Molecules in a Non-Hydrocolloid. *Int. Nano Lett.* **2013**, *3*, 1–7.
75. Zhang, X. D.; Wu, D.; Shen, X.; Liu, P. X.; Yang, N.; Zhao, B.; Zhang, H.; Sun, Y. M.; Zhang, L. A.; Fan, F. Y. Size-Dependent *in Vivo* Toxicity of PEG-Coated Gold Nanoparticles. *Int. J. Nanomed.* **2011**, *6*, 2071–2081.
76. Song, W.; Wang, F.; Lotfi, P.; Sardiello, M.; Segatori, L. 2-Hydroxypropyl-beta-Cyclodextrin Promotes Transcription Factor EB-Mediated Activation of Autophagy: Implications for Therapy. *J. Biol. Chem.* **2014**, *289*, 10211–10222.
77. Gorski, S. M.; Chittaranjan, S.; Pleasance, E. D.; Freeman, J. D.; Anderson, C. L.; Varhol, R. J.; Coughlin, S. M.; Zuyderduyn, S. D.; Jones, S. J.; Marra, M. A. A Sage Approach to Discovery of Genes Involved in Autophagic Cell Death. *Curr. Biol.* **2003**, *13*, 358–363.
78. Lee, C. Y.; Clough, E. A.; Yellon, P.; Teslovich, T. M.; Stephan, D. A.; Baehrecke, E. H. Genome-Wide Analyses of Steroid- and Radiation-Triggered Programmed Cell Death in Drosophila. *Curr. Biol.* **2003**, *13*, 350–357.
79. Levine, B.; Yuan, J. Autophagy in Cell Death: An Innocent Convict? *J. Clin. Invest.* **2005**, *115*, 2679–2688.
80. Kroemer, G.; Jaattela, M. Lysosomes and Autophagy in Cell Death Control. *Nat. Rev. Cancer* **2005**, *5*, 886–897.
81. Wang, F.; Song, W.; Brancati, G.; Segatori, L. Inhibition of Endoplasmic Reticulum-Associated Degradation Rescues Native Folding in Loss of Function Protein Misfolding Diseases. *J. Biol. Chem.* **2011**, *286*, 43454–43464.
82. Bacus, S. S.; Gudkov, A. V.; Lowe, M.; Lyass, L.; Yung, Y.; Komarov, A. P.; Keyomarsi, K.; Yarden, Y.; Seger, R. Taxol-Induced Apoptosis Depends on Map Kinase Pathways (ERK and P38) and Is Independent of P53. *Oncogene* **2001**, *20*, 147–155.
83. Asati, A.; Santra, S.; Kaittanis, C.; Perez, J. M. Surface-Charge-Dependent Cell Localization and Cytotoxicity of Cerium Oxide Nanoparticles. *ACS Nano* **2010**, *4*, 5321–5331.
84. Lieberman, A. P.; Puertollano, R.; Raben, N.; Slaugenhaupt, S.; Walkley, S. U.; Ballabio, A. Autophagy in Lysosomal Storage Disorders. *Autophagy* **2012**, *8*, 719–730.
85. Vazquez, C. L.; Colombo, M. I. Assays to Assess Autophagy Induction and Fusion of Autophagic Vacuoles with a Degradative Compartment, Using Monodansylcadaverine (MDC) and DQ-BSA. *Methods Enzymol.* **2009**, *452*, 85–95.
86. Gonzalez-Noriega, A.; Grubb, J. H.; Talkad, V.; Sly, W. S. Chloroquine Inhibits Lysosomal Enzyme Pinocytosis and Enhances Lysosomal Enzyme Secretion by Impairing Receptor Recycling. *J. Cell Biol.* **1980**, *85*, 839–852.
87. Kabeya, Y.; Mizushima, N.; Ueno, T.; Yamamoto, A.; Kirisako, T.; Noda, T.; Kominami, E.; Ohsumi, Y.; Yoshimori, T. LC3, a Mammalian Homologue of Yeast Apg8p, Is Localized in Autophagosome Membranes after Processing. *EMBO J.* **2000**, *19*, 5720–5728.
88. Mizushima, N.; Yamamoto, A.; Matsui, M.; Yoshimori, T.; Ohsumi, Y. *In Vivo* Analysis of Autophagy in Response to Nutrient Starvation Using Transgenic Mice Expressing a Fluorescent Autophagosome Marker. *Mol. Biol. Cell* **2004**, *15*, 1101–1111.
89. Mizushima, N.; Yoshimori, T.; Levine, B. Methods in Mammalian Autophagy Research. *Cell* **2010**, *140*, 313–326.
90. Eskelinen, E.-L.; Tanaka, Y.; Saftig, P. At the Acidic Edge: Emerging Functions for Lysosomal Membrane Proteins. *Trends Cell Biol.* **2003**, *13*, 137–145.
91. Albanese, A.; Chan, W. C. Effect of Gold Nanoparticle Aggregation on Cell Uptake and Toxicity. *ACS Nano* **2011**, *5*, 5478–5489.
92. Jokerst, J. V.; Khademi, C.; Gambhir, S. S. Intracellular Aggregation of Multimodal Silica Nanoparticles for Ultrasound-Guided Stem Cell Implantation. *Sci. Transl. Med.* **2013**, *5*, 177ra35.
93. dos Santos, T.; Varela, J.; Lynch, I.; Salvati, A.; Dawson, K. A. Effects of Transport Inhibitors on the Cellular Uptake of Carboxylated Polystyrene Nanoparticles in Different Cell Lines. *PLoS One* **2011**, *6*, e24438.
94. Halamoda Kenzaoui, B.; Chapuis Bernasconi, C.; Guney-Ayra, S.; Juillerat-Jeanneret, L. Induction of Oxidative Stress, Lysosome Activation and Autophagy by Nanoparticles in Human Brain-Derived Endothelial Cells. *Biochem. J.* **2012**, *441*, 813–821.
95. Neibert, K. D.; Maysinger, D. Mechanisms of Cellular Adaptation to Quantum Dots—the Role of Glutathione and Transcription Factor EB. *Nanotoxicology* **2012**, *6*, 249–262.
96. Vevers, W. F.; Jha, A. N. Genotoxic and Cytotoxic Potential of Titanium Dioxide (TiO_2) Nanoparticles on Fish Cells *in Vitro*. *Ecotoxicology* **2008**, *17*, 410–420.
97. Sohaebuddin, S. K.; Thevenot, P. T.; Baker, D.; Eaton, J. W.; Tang, L. P. Nanomaterial Cytotoxicity Is Composition, Size, and Cell Type Dependent. *Part. Fibre Toxicol.* **2010**, 10.1186/1743-8977-7-22.
98. Oh, N.; Park, J. H. Endocytosis and Exocytosis of Nanoparticles in Mammalian Cells. *Int. J. Nanomed.* **2014**, *9* (Suppl 1), 51–63.
99. Sakhtianchi, R.; Minchin, R. F.; Lee, K. B.; Alkilany, A. M.; Serpooshan, V.; Mahmoudi, M. Exocytosis of Nanoparticles from Cells: Role in Cellular Retention and Toxicity. *Adv. Colloid Interface Sci.* **2013**, *201*, 18–29.
100. Futerman, A. H.; van Meer, G. The Cell Biology of Lysosomal Storage Disorders. *Nat. Rev. Mol. Cell Biol.* **2004**, *5*, 554–565.
101. Hassan, A. A.; Chan, B. T. Y.; Tran, L. A.; Hartman, K. B.; Ananta, J. S.; Mackeyev, Y.; Hu, L. Y.; Pautler, R. G.; Wilson, L. J.; Lee, A. V. Serine-Derivatized Gadonanotubes as Magnetic Nanoprobes for Intracellular Labeling. *Contrast Media Mol. Imaging* **2010**, *5*, 34–38.
102. Wang, F.; Chou, A.; Segatori, L. Lacidipine Remodels Protein Folding and Ca^{2+} Homeostasis in Gaucher's

Disease Fibroblasts: A Mechanism to Rescue Mutant Glucocerebrosidase. *Chem. Biol.* **2011**, *18*, 766–776.
103. Vandesompele, J.; De Preter, K.; Pattyn, F.; Poppe, B.; Van Roy, N.; De Paepe, A.; Speleman, F. Accurate Normalization of Real-Time Quantitative RT-PCR Data by Geometric Averaging of Multiple Internal Control Genes. *Genome Biol.* **2002**, *3*, RESEARCH0034.
104. Wang, F.; Segatori, L. Remodeling the Proteostasis Network to Rescue Glucocerebrosidase Variants by Inhibiting Er-Associated Degradation and Enhancing ER Folding. *PLoS One* **2013**, *8*, e61418.